ACS APPLIED MATERIALS & INTERFACES

Research Article

www.acsami.org

Polarity and Air-Stability Transitions in Field-Effect Transistors Based on Fullerenes with Different Solubilizing Groups

Hojeong Yu,[†,‡] Han-Hee Cho,[‡,§] Chul-Hee Cho,[§] Ki-Hyun Kim,[§] Dong Yeong Kim,[†] Bumjoon J. Kim,*[,§] and Joon Hak Oh*[,†]

[†]School of Nano-Bioscience & Chemical Engineering, KIER-UNIST Advanced Center for Energy, Low Dimensional Carbon Materials Center, Ulsan National Institute of Science and Technology (UNIST), Ulsan 689-798, Korea

[§]Department of Chemical and Biomolecular Engineering, Korea Advanced Institute of Science and Technology (KAIST), Daejeon 305-701, Korea

Supporting Information

ABSTRACT: A series of *o*-xylene and indene fullerene derivatives with varying frontier molecular orbital energy levels were utilized for assessing the impact of the number of solubilizing groups on the electrical performance of fullerene-based organic-field-effect transistors (OFETs). The charge-carrier polarity was found to be strongly dependent upon the energy levels of fullerene derivatives. The *o*-xylene C_{60} monoadduct (OXCMA) and indene C_{60} monoadduct (ICMA) exhibited unipolar *n*-channel behaviors with high electron mobilities, whereas the bis- and trisadducts of indene and *o*-xylene C_{60} derivatives showed ambipolar charge transport. The OXCMA OFETs fabricated by solution shearing and molecular *n*-type doping showed an electron mobility of up to 2.28 $cm^2\ V^{-1}\ s^{-1}$, which is one of the highest electron mobilities obtained from solution-processed fullerene thin-film devices. Our findings systematically demonstrate the relationship between the energy level and charge-carrier polarity and provide insight into molecular design and processing strategies toward high-performance fullerene-based OFETs.

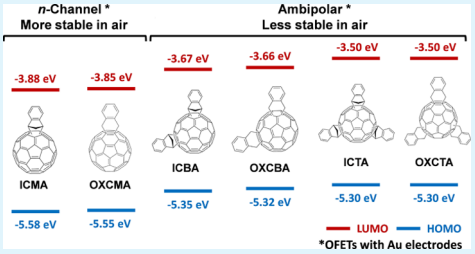

KEYWORDS: *fullerene, organic-field-effect transistor, solubilizing groups, n-type doping, molecular design*

INTRODUCTION

Organic field-effect transistors (OFETs) have been actively explored as promising candidates for flexible low-cost electronic device applications. While *p*-channel organic semiconductors have been studied extensively, *n*-channel organic semiconductors have been less exploited because of the vulnerability of electrons to being trapped by environmental oxidants upon exposure to air. However, to make full use of the organic circuitry, it is essential to combine *p*-channel transistors with *n*-channel transistors for the fabrication of organic complementary circuits because they offer lower power dissipation, greater operating speed, and higher stability in comparison to unipolar circuits. In addition, there is a rapidly growing demand for *n*-channel semiconductors in various applications such as p−n junctions, bipolar transistors, and novel acceptor materials in organic solar cells. Despite the recent advances in the development of *n*-channel organic semiconductors,[1−6] the availability of air-stable high-mobility *n*-channel semiconductors is still limited compared to *p*-channel materials.

Fullerene derivatives including [6,6]phenyl-C_{61}-butyric acid methyl ester (PCBM)[7] have been frequently used as electron-transporting materials in organic solar cells[8−11] and OFETs.[12−14] In recent years, much effort has been directed toward the development of fullerene derivatives that can be solution-processed, resulting in higher electron mobility,[15−18] air stability,[15,19,20] desired molecular packing, and orientation[15,16,18−20] in fullerene-based *n*-channel OFETs. Much of the previous research on soluble fullerene derivatives has focused on diversifying monosubstitution groups and assessing their effects on the electrical performance[15−20] and air stability[19,20] of OFETs. To the best of our knowledge, little attention has been paid to the systematic study of the effects of the number of solubilizing groups attached to the fullerene backbone moiety. In particular, the study of the effects of the frontier molecular orbital energy levels of fullerene derivatives on the polarity and air stability of the resulting OFETs has been largely left untouched.

Herein we investigate the effects of the number of solubilizing groups and structural differences of fullerene adducts on the charge-transport properties and air stability using a series of *o*-xylenyl C_{60} mono-, bis-, and trisadducts (OXCMA, OXCBA, and OXCTA, respectively)[21,22] and indene C_{60} multiadducts including indene C_{60} mono-, bis-, and trisadducts (ICMA, ICBA, and ICTA, respectively).[23−27] The thin films of the fullerene derivatives were prepared using a solution-shearing technique.[28−30] The charge-carrier polarity and air stability of the OFETs based on these fullerene derivatives were systematically investigated by analyzing the

Received: February 18, 2013
Accepted: May 15, 2013
Published: May 15, 2013

   dx.doi.org/10.1021/am400618r | ACS Appl. Mater. Interfaces 2013, 5, 4865−4871

current−voltage (I−V) characteristics. Interestingly, the ICMA- and OXCMA-based transistors exhibited much higher air stability in comparison with PCBM-based transistors. The molecular packing and morphology of the fullerene mono-adduct thin films were also investigated. Furthermore, we report the effects of molecular n-type doping on the device performance, using [4-(1,3-dimethyl-2,3-dihydro-1H-benzoimidazol-2-yl)-phenyl]dimethylamine (N-DMBI) as the n-type dopant,[31−34] which resulted in a high electron mobility of 2.28 $cm^2\ V^{-1}\ s^{-1}$.

EXPERIMENTAL SECTION

Materials and Instrumentation. All commercially available reagents were used without further purification. The organic solvents were used as anhydrous solvents. Analytical thin-layer chromatography was performed using Merck silica gel 60 F254 precoated plates (0.25 mm) with a fluorescent indicator. Flash column chromatography was carried out on Merck silica gel 60 (230−400 mesh). Matrix-assisted laser desorption ionization time-of-flight (MALDI-TOF) mass spectra were recorded on a Bruker autoflex III mass spectrometer. Elemental analysis was performed with a ThermoQuest Italia SPA model EA1110-FISONS. UV−vis absorption spectra were obtained using a Shimadzu UV−vis−near-IR 3600 spectrophotometer. Cyclic voltammetry (CV) curves were measured using a CHI 600C electrochemical analyzer. The CV curves of the different fullerene derivatives were collected at room temperature using a conventional three-electrode system (platinum disk working electrode, platinum wire counter electrode, and silver wire quasi-reference electrode) in a 0.1 M tetrabutylammonium tetrafluoroborate (NBu_4BF_4) solution in o-dichlorobenzene at a potential scan rate of 10 mV s^{-1}. The reduction potentials of the solutions of fullerene derivatives against the silver quasi-reference electrode were measured and calibrated against a ferrocene/ferrocenium (Fc/Fc^+) redox couple, assuming that the absolute energy level of Fc/Fc^+ was −4.80 eV.

Preparation of Indene and o-Xylenyl C_{60} Multiadducts. A series of indene and o-xylene C_{60} multiadducts were synthesized using the [4 + 2] cycloaddition reaction between C_{60}-fullerene and corresponding adducts. All fullerene derivatives were synthesized according to the reported procedure.[21,23] The synthesized derivatives were isolated through column chromatography and confirmed by MALDI-TOF mass spectrometry and elemental analysis.

Surface Modification of Device and Shearing Substrates. Heavily n-doped silicon wafers (<0.004 Ω cm) with a 300-nm-thick SiO_2 dielectric (C_i = 10 nF cm^{-2}) were used as substrates for OFETs. The SiO_2/Si surface was treated with n-octadecyltrimethoxysilane (OTS) in the solution phase.[35] These wafers were first cleaned by a piranha solution (70:30 H_2SO_4/H_2O_2 by vol %) for 20 min and then thoroughly rinsed in deionized water followed by N_2 gun blowing. The SiO_2/Si substrates were treated with UV-ozone plasma for 15 min. For OTS treatment, the cleaned substrates were spin-coated with a 3 mM solution of OTS in trichloroethylene and then placed in a desiccator under vaporized ammonium hydroxide for 12 h at room temperature. The modified substrates were ultrasonicated with toluene and rinsed sequentially with toluene, acetone, and isopropyl alcohol, followed by drying with N_2 blowing.

OFET Fabrication and Testing. In a typical solution-shearing process, the films were deposited onto the OTS-treated SiO_2/Si substrates using chlorobenzene solutions (3 mg mL^{-1}) of the fullerene derivatives. An upper substrate dragged the placed solution on a heated substrate at a shearing rate of 0.12 mm s^{-1}, which was controlled by a digital syringe pump. For comparison, drop-cast thin films were also prepared on the OTS-modified SiO_2/Si substrates. All of the semiconductor films prepared were then placed in a vacuum oven at 80 °C for complete drying. After drying, 40 nm gold electrodes were thermally evaporated through a shadow mask onto the semiconductor layer. The current−voltage (I−V) characteristics of the devices were measured either in a N_2-filled glovebox or in air conditions using a Keithley 4200 semiconductor parametric analyzer. Air-stability tests of OFET devices were carried out in the dark with humidity and temperature maintained at ∼40% and ∼21 °C, respectively. Each device was assessed from the transfer characteristics as a function of the exposure time in air. The field-effect mobility was calculated in the saturation regime using the following equation:

$$I_D = \frac{W}{2L}\mu C_i(V_G - V_T)^2$$

where I_D is the drain current, W and L are the semiconductor channel width and length, respectively, μ is the mobility, C_i is the capacitance per unit area of the gate dielectric, and V_G and V_T are the gate voltage and threshold voltage, respectively.

RESULTS AND DISCUSSION

Chemical Structures and Energy Levels of Fullerene Derivatives. To investigate the effect of the number of solubilizing groups in the fullerene backbone on the field-effect mobility, six fullerene derivatives were synthesized according to the method described in the literature with different numbers of indene and o-xylene groups (ranging from 1 to 3).[21,23] The chemical structures and frontier molecular orbital energy levels of the synthesized fullerene derivatives are shown in Figure 1.

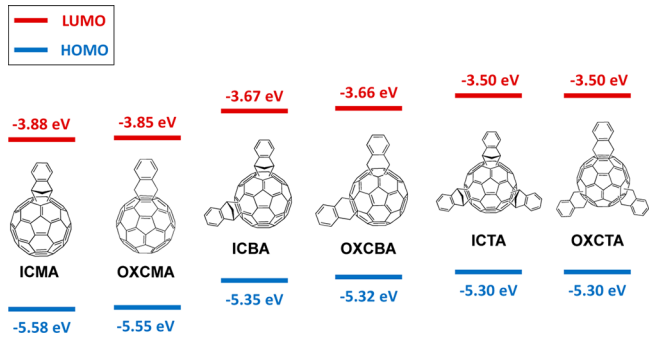

Figure 1. Chemical structures with HOMO and LUMO energy levels of indene C_{60} multiadducts and o-xylenyl C_{60} multiadducts.

The lowest unoccupied molecular orbital (LUMO) energy levels of the six different fullerene derivatives were estimated using CV measurements (Figure S6 in the Supporting Information, SI). ICMA, ICBA, and ICTA showed LUMO energy levels of −3.88, −3.67, and −3.50 eV, respectively. Similarly, OXCMA, OXCBA, and OXCTA exhibited energy levels of −3.85, −3.66, and −3.50 eV, respectively. As the number of solubilizing groups increased, the LUMO energy levels increased gradually. Because the solubilizing groups on the fullerene derivatives were combined with the fullerene core, the number of sp^2 carbons in the fullerene molecules reduced with an increase in the number of solubilizing groups, resulting in a decrease in the electron affinity.[21,23] The LUMO levels of these fullerene derivatives corresponded to the empirical LUMO windows of n-channel organic semiconductors that fall under the air-unstable (LUMO > −3.8 eV) or on-set region (−3.8 to −4.0 eV) of air stability with respect to gold electrodes.[36−38] The highest occupied molecular orbital (HOMO) energy levels of the indene C_{60} derivatives were estimated to be −5.58, −5.35, and −5.30 eV based on the difference between the LUMO level and the optical bandgap of each of the fullerene derivatives measured by the absorption onset of the UV−vis absorption spectra (Figure S7 in the SI). Similarly, the HOMO levels of OXCMA, OXCBA, and OXCTA were found to be −5.55, −5.32, and −5.30 eV, respectively. As the number of solubilizing groups increased,

Table 1. Electrical Performance of OFET Devices Based on the Solution-Sheared Thin Films of Fullerene Derivatives[a]

	n-type				*p*-type			
compound	$\mu_{e,max}$ [cm^2 V^{-1} s^{-1}][b]	$\mu_{e,avg}$ [cm^2 V^{-1} s^{-1}][c]	I_{on}/I_{off}	V_T [V]	$\mu_{h,max}$ [cm^2 V^{-1} s^{-1}]	$\mu_{h,avg}$ [cm^2 V^{-1} s^{-1}]	I_{on}/I_{off}	V_T [V]
OXCMA	0.514	0.161	1.0×10^4	5.7	N/A[d]	N/A	N/A	N/A
OXCBA	1.20×10^{-3}	3.88×10^{-4}	1.1×10^5	20.9	2.74×10^{-5}	3.93×10^{-6}	1.2×10^2	−42.4
OXCTA	2.01×10^{-4}	2.58×10^{-5}	8.5×10^1	0.5	6.59×10^{-5}	2.88×10^{-5}	2.6×10^2	−2.1
ICMA	0.0704	0.0676	2.3×10^5	24.2	N/A	N/A	N/A	N/A
ICBA	6.31×10^{-3}	3.50×10^{-3}	9.3×10^3	38.1	1.62×10^{-5}	1.38×10^{-5}	3.8×10^3	−56.3
ICTA	4.50×10^{-6}	2.13×10^{-6}	2.9×10^3	51.2	1.26×10^{-5}	1.16×10^{-5}	1.3×10^4	−30.5

[a]The *I*−*V* characteristics were measured in a N_2-filled glovebox. [b]The maximum mobility of the OFET devices. [c]The average mobility of the OFET devices. [d]The *p*-type performance of fullerene monoadducts was not observed.

the HOMO levels also increased gradually. The HOMO and LUMO levels of all of the fullerene derivatives are summarized in Table S1 in the SI.

OFET Performance. To evaluate the field-effect mobility of the fullerene derivatives, we fabricated OFETs with top-contact bottom-gate geometry. The thin films based on the fullerene derivatives were prepared by either solution shearing[29] or drop casting of the solution onto OTS-treated SiO_2/Si substrates. In the solution-shearing method, a small volume of an organic semiconductor solution is placed between two preheated silicon wafers that move relative to each other at a controlled rate. This method yields crystalline and aligned thin films along the shearing direction, and thus OFETs of various small molecules prepared through the solution-shearing process show mobilities that are comparable and often superior to the values shown by devices obtained by drop casting.[28,30] A recent in-depth study by Giri et al. revealed that the lattice strain achieved by solution shearing is highly beneficial in achieving an increased charge-transfer integral of π planes and allows for efficient charge transport.[29] Further experimental details are described in the Experimental Section. The effects of the number of adducts on the electrical performance were investigated by carrying out *I*−*V* measurements in a glovebox filled with N_2 gas. The *I*−*V* characteristics of the OFETs obtained from the solution-sheared and drop-cast thin films of all of the fullerene derivatives are summarized in Tables 1 and S2 in the SI, respectively. The electron mobilities of the solution-sheared films were comparatively higher than those of the drop-cast films, which is consistent with the general trend observed for other small-molecule-based OFETs.[28−30] The OFETs based on fullerene monoadducts of both indene and *o*-xylene C_{60} derivatives showed the best performance. Figure 2 shows the transfer and output characteristics of the OFETs based on solution-sheared OXCMA and ICMA. The OXCMA devices exhibited a maximum electron mobility (μ_e) of 0.514 cm^2 V^{-1} s^{-1} at a shearing rate of 0.12 mm s^{-1}, which is relatively higher than the electron mobilities shown by solution-processed fullerene thin-film devices.[15−18] Interestingly, the fullerene monoadducts showed relatively more air-stable field-effect-transistor behavior than PCBM, which will be discussed in the following section.

Further, the fullerene multiadducts with indene and *o*-xylene C_{60} derivatives exhibited ambipolar behaviors; i.e., both electron- and hole-transporting properties were observed (Figures S1 and S2 in the SI). This is presumably because of the decreased injection barriers for holes as well as the increased injection barriers for electrons with respect to the gold contacts. Our findings on the *p*-channel operation of fullerene multiadducts are noteworthy because only the *n*-channel operation has been observed from ICBA OFETs with Ca/Al electrodes.[39]

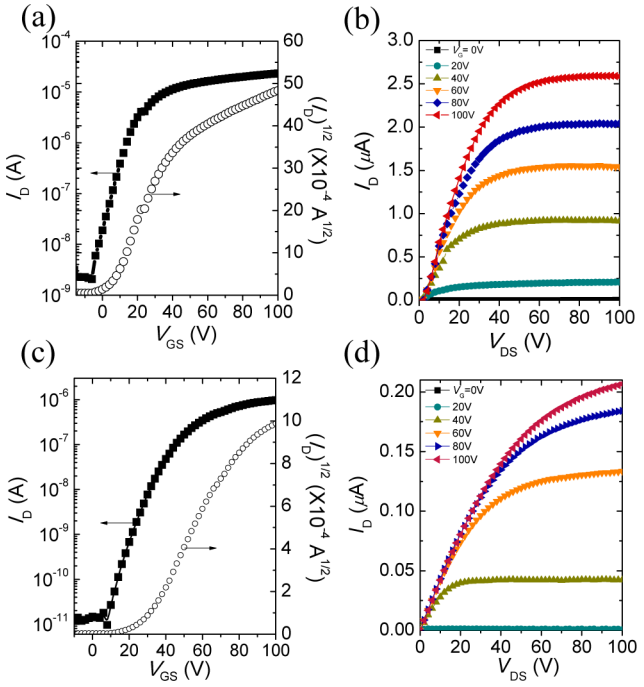

Figure 2. OFET performance of solution-sheared (a and b) *o*-xylene C_{60} monoadduct (OXCMA; W/L = 16.64) and (c and d) indene C_{60} monoadduct (ICMA; W/L = 5.37) devices. For parts a and c, the transfer curves were recorded at V_{DS} = +100 V, and for parts b and d, the output curves were recorded with increasing V_{GS} in steps of 20 V from 0 to +100 V.

Air Stability. In *n*-channel OFETs, electron carriers run the risk of being trapped by ambient oxidants.[38] Therefore, in addition to ensuring high electron mobility, it is important to develop air-stable *n*-channel organic semiconductors. The fullerene monoadducts exhibited relatively higher field-effect mobility and air stability compared to fullerene bis- and trisadducts, which can possibly be ascribed to the energetically low-lying LUMO levels and the closely packed molecules in the thin-film state. The relationship of the electron affinity and air stability for various *n*-channel OFETs has been studied extensively.[20,36,37,40−43] The energetics-based interpretation of ambient carrier instability in *n*-type-doped conducting polymers was initially reported by de Leeuw et al.[41] Combining the solution-phase electrochemical potentials related to water and oxygen molecules, Jones et al. reported the thermodynamic (i.e., reduction potential) requirements for the air-stable *n*-channel operation of arylenebisimides.[36] In addition, Antho-

poulos et al. have suggested a reduction potential window for air stability of C_{60} and C_{70} derivatives as LUMOs ≤ -4 eV.[40] The LUMO levels of the fullerene monoadduct films are close to the empirical reduction potential window. Another possible explanation for the air stability of negative charge carriers lies in the formation of kinetic barriers that prevent diffusion of ambient oxidants into the active channel area.[44] It has also been stressed that considering the interplay between multiple thermodynamic and kinetic factors is of importance for understanding the ambient stability of *n*-channel OFETs.[38] Several research groups have reported the correlation between the crystallinity of fullerene films and their air stability.[15,20] According to these previous works, fullerene derivatives can show air stability due to the introduction of substituent groups, which enables close packing in the molecular structure, whereby oxygen and water molecules cannot easily diffuse into the channel.[15] Moreover, it has been recently reported that molecular *n*-type doping is an efficient method to significantly improve the air stability of *n*-channel OFETs by compensating for the trapped electron carriers in ambient conditions.[34,45,46]

The air stability of OFETs based on fullerene monoadducts was measured by monitoring their electrical properties as a function of the exposure time. The measurements were carried out in ambient air under ~40% humidity at room temperature. The air stability of PCBM OFETs was also recorded for comparison. Figure 3 presents variations in the field-effect

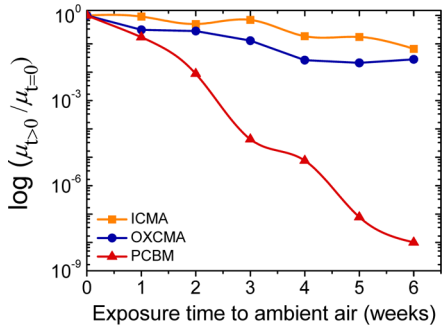

Figure 3. Air-stability test of OFETs based on fullerene derivatives. Saturation mobility (V_{DS}= +100 V) as a function of the atmospheric exposure time ($\mu_{t>0}$) normalized to the mobility measured under ambient air conditions ($\mu_{t=0}$). The relative humidity in ambient air was approximately 40%. The electron mobilities of the initial devices based on OXCMA, ICMA, and PCBM thin films were 0.041, 0.051, and 0.033 $cm^2\ V^{-1}\ s^{-1}$ with *W*/*L* values of 10.16, 4.41, and 14.20, respectively.

mobility as a function of the exposure time. The electron mobilities of the initial devices based on OXCMA, ICMA, and PCBM thin films were 0.041, 0.051, and 0.033 $cm^2\ V^{-1}\ s^{-1}$, respectively. OFETs based on fullerene bis- and trisadducts could operate only in a N_2 atmosphere. Interestingly, the OXCMA- and ICMA-based OFETs exhibited relatively air-stable operation showing degradation in the mobility by only 1 order of magnitude after 6 weeks. However, the PCBM-based OFETs showed rapid performance degradation by greater than 8 orders of magnitude.

Judging from the correlation of empirical LUMO windows and the air stability of *n*-channel semiconductors, the LUMO energy levels of ICMA (−3.88 eV) and OXCMA (−3.85 eV) fall under the air-unstable or on-set region of air stability with respect to gold contacts. This discrepancy in the thermodynamic considerations may be caused by the difference between the actual LUMO level in the solid thin-film state and that of the single molecule in the solution state. Because electron coupling exists between molecules in crystalline solids, LUMO levels measured by CV could be higher than the actual LUMO levels of the materials tested in the solid state.[38,47−49] The differences in the air stabilities of PCBM and ICMA or OXCMA can be explained on the basis of their chemical structures. PCBM contains a three-membered ring between the adduct and the C_{60} bulky ball, while ICMA and OXCMA contain the more stable six-membered ring formed by the [4 + 2] cycloaddition reaction.[7,21,23,50] Therefore, compared to PCBM, ICMA and OXCMA show a lesser tendency to react with oxygen or water molecules in air. The other possible reason for their air stability can be the kinetic blocking mechanism operating against the diffusion of environmental oxidants into the channel by the effective packing of molecules by the monosubstituent. To confirm this, X-ray diffraction (XRD) analysis was performed to shed light on the relationship between the molecular ordering of the fullerene monoadducts and air stability using drop-cast thin films with similar thicknesses (~1.5 μm). ICMA and OXCMA thin films exhibited well-defined strong XRD peaks, indicating the presence of highly ordered microstructures in the films (Figure S3 and Table S3 in the SI). However, OXCMA films showed a strong primary diffraction peak at 2θ = 5.23°, corresponding to a *d* spacing of 16.86 Å. The presence of another strong peak at 2θ = 6.19° (*d* spacing =14.26 Å) indicated the existence of crystalline polymorphs in the OXCMA film.[51] Higher-order diffraction peaks of the primary crystalline phase were observed at 2θ = 10.46°, 15.69°, and 20.99°, corresponding to the second-, third-, and fourth-order diffractions. This indicates that the thin film has a relatively long-range order. The ICMA films showed two closely spaced diffraction peaks at 2θ = 8.52° and 8.88° (*d* spacing =10.37 and 9.95 Å, respectively). In contrast, the drop-cast PCBM film prepared under the same conditions showed ill-defined and weak diffraction patterns.

Molecular n-Type Doping and Shearing Rate Control. Among the tested fullerene derivatives, the maximum electron mobility was obtained from the solution-sheared OXCMA film. To improve the performance of the OXCMA OFETs further, we intentionally added an *n*-type dopant, N-DMBI,[52] to the OXCMA solution during the solution-shearing process. This was done with a view of enhancing the electron mobility and air stability by increasing the density of mobile electrons.[34] Controlled molecular *n*-type doping is known to increase negative charge-carrier densities.[32,34,45,46,53−56] In particular, the dopant concentration is a critical issue for the fabrication of high-performance OFETs because the dopant can act as an impurity element that deteriorates the molecular packing of the semiconductors. In addition, excessively high doping levels lead to low on/off current ratios because of the elevated off current. In our experiment, the field-effect mobility of N-DMBI-doped-OXCMA OFETs obtained by solution processing was effectively enhanced by carefully controlling the doping concentration to 0.2 wt %, while maintaining the high on/off current ratio. The chlorobenzene solution containing N-DMBI and OXCMA was used for solution shearing. In order to effectively activate the *n*-type dopant, the solution-sheared films were placed on a hot plate at 80 °C overnight under a N_2 atmosphere.[34] The LUMO level (−3.85 eV) of OXCMA is much higher than the HOMO level of N-DMBI (−4.67 eV), implying that electron transfer from N-DMBI to OXCMA cannot occur spontaneously. However, mild heating of N-

DMBI at 80 °C causes the removal of hydrogen and produces the neutral N-DMBI radical. The singly occupied molecular orbital (SOMO) level of the neutral radical is estimated to be −2.36 eV,[34] which implies that the neutral radicals can effectively act as *n*-type dopants.

The highly crystalline OXCMA microribbons were successfully fabricated by changing the solution concentration from 3 to 10 mg mL^{-1} and the shearing rate from 0.12 to 0.2 mm s^{-1}. Atomic force microscopy (AFM) topography images of the solution-sheared films showed ribbon-like morphologies with fewer grain boundaries in samples obtained at higher shearing speed (Figure 4). The crystalline microribbon structures

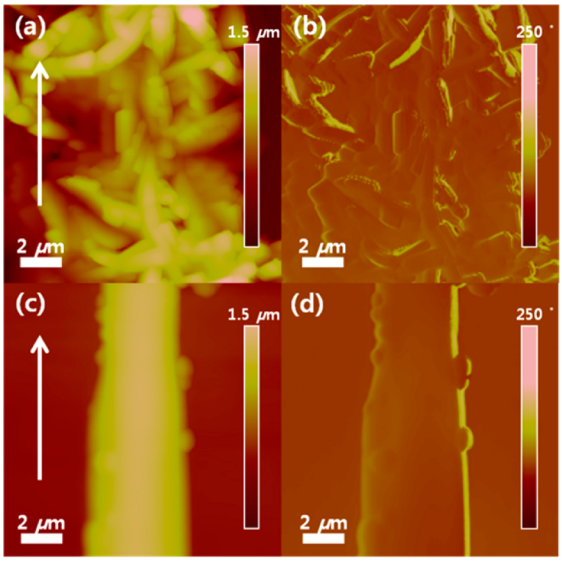

Figure 4. AFM topographic height (left) and phase (right) images of solution-sheared OXCMA films formed at a shearing rate of (a and b) 0.12 mm s^{-1} and (c and d) 0.2 mm s^{-1} on OTS-treated SiO_2/Si substrates. The arrow indicates the direction of shearing.

obtained at higher shearing rates displayed fewer grain boundaries compared to structures in the drop-cast film (Figure S4 in the SI). XRD analysis of the solution-sheared OXCMA film (obtained at a shearing rate of 0.12 mm s^{-1}) exhibited four distinct XRD peaks at equal intervals, with the primary peak occurring at 2θ = 5.25°, corresponding to a *d* spacing of 16.83 Å (Figure S5a in the SI). The peak assignment data of the solution-sheared OXCMA are presented in Table S4 in the SI. In the solution-sheared film, the polymorphic peak at 2θ = 6.19° observed from the OXCMA drop-cast film disappeared, indicating a higher degree of purity in the crystalline thin film. The higher-order diffraction peaks were also observed at 2θ = 10.47°, 15.75°, and 20.93°, corresponding to (002), (003), and (004) peaks, respectively. The film obtained by solution shearing at a rate of 0.2 mm s^{-1} (with a similar thickness of ∼1.5 μm) exhibited very strong diffraction peaks with a narrow full width at half-maximum at identical 2θ positions (Figure S5b in the SI). This indicated that the increased shearing rate resulted in an increase in the crystallinity of the OXCMA film. During the solution-shearing process, an OTS-treated top shearing plate dragged the solution across the OTS-treated bottom substrate to induce highly crystalline and aligned films. By combining solution shearing with *n*-type doping, we obtained an average electron mobility of 1.43 ± 0.85 $cm^2\ V^{-1}\ s^{-1}$ for the OXCMA film. The average electron mobility of the *n*-type-doped devices was 9 times higher than that of the devices based on solution-sheared pure OXCMA thin films (0.161 $cm^2\ V^{-1}\ s^{-1}$) with the V_T negatively shifted by 23.7 V. This indicated that the devices became easier to turn on because of the *n*-type doping effect.[34] The maximum electron mobility was 2.28 $cm^2\ V^{-1}\ s^{-1}$, which is among the highest electron mobilities obtained from solution-processed fullerene thin films, to the best of our knowledge. The transfer and output characteristics of the device that performed the best are shown in Figure 5. To further demonstrate the effect of *n*-

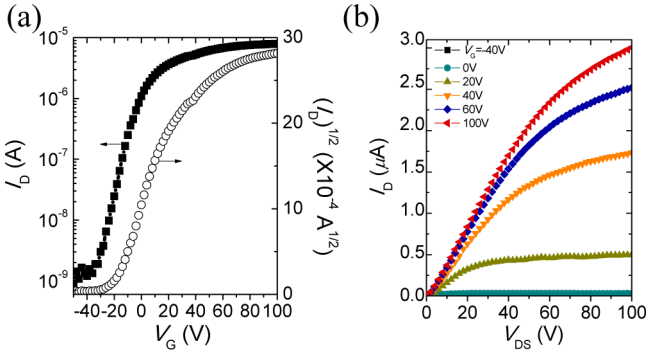

Figure 5. OFET performance of a solution-sheared N-DMBI-doped-OXCMA device (W/L = 0.61): (a) I_D–V_{GS} characteristic recorded with V_{DS} = +100 V and (b) I_D–V_{DS} characteristic with increasing V_{GS} in steps of 20 V from 0 to +100 V.

type doping with N-DMBI, we also compared the device performance of the doped and undoped films obtained by spin coating. The electrical performances of the spin-coated doped and pure OFETs are compared in Figure 6. It can be seen that

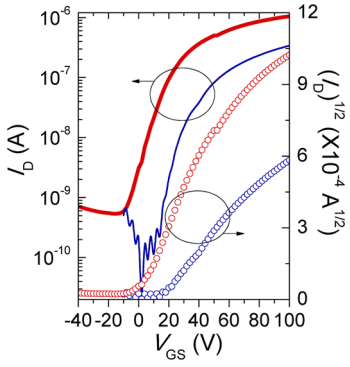

Figure 6. OFET performance of a spin-coated pure OXCMA field-effect transistor (blue line) and an N-DMBI-doped-OXCMA field-effect transistor (red line). The I_D–V_{GS} characteristics were recorded with V_{DS} = +100 V. Both OFET devices had a channel length (L) of 50 μm, with a W/L value of 20.

the electron mobility was increased by 4.4 times for the N-DMBI-doped OXCMA OFETs. The negatively shifted V_T of the doped device indicates that the doped device can be turned on easily. Besides the doping effect, each of the two parameters (i.e., the change in the solution concentration from 3 to 10 mg mL^{-1} and the shearing rate from 0.12 to 0.2 mm s^{-1}) by itself enhanced the device performance by around 2 times compared to the device obtained using films formed under other identical conditions (Figures S8 and S9 in the SI). Our finding demonstrates a viable way of achieving air-stable high-mobility

n-channel OFETs, which combines molecular *n*-type doping with solution shearing.

CONCLUSIONS

In conclusion, we have investigated the effect of the number of solubilizing groups attached to the fullerene backbone on the OFET performance. Fullerene monoadducts showed *n*-type field-effect behaviors with respect to gold contacts, while bis- and trisadducts exhibited ambipolar behaviors with relatively well-balanced hole and electron mobilities. Fullerene monoadducts for each group of indene and *o*-xylene C_{60} derivatives showed the best performance with the solution-shearing process. Long-term air stability was observed in fullerene monoadduct OFETs, while PCBM OFETs degraded rapidly. The results were reasoned based on thermodynamic and kinetic considerations. By optimizing the doping level and shearing conditions, electron mobility as high as 2.28 $cm^2\ V^{-1}\ s^{-1}$ was achieved from the N-DMBI-doped-OXCMA OFETs. Fewer structural defects in the crystalline films induced effectively continuous pathways for charge transport.[57] The processing strategies comprising solution shearing and molecular *n*-type doping led to the successful fabrication of high-performance *n*-channel OFETs. Our findings may provide insight into considering thermodynamic and kinetic factors that affect the polarity and air-stability behaviors of fullerene derivatives, providing guidelines for molecular design.

ASSOCIATED CONTENT

Supporting Information

CV curves and UV−vis absorption spectra of the indene and *o*-xylene C_{60} multiadducts and PCBM, *I*−*V* characteristics of fullerene bis- and trisadducts, XRD patterns of drop-cast PCBM, OXCMA, and ICMA films and of solution-sheared OXCMA films, AFM topographic images of drop-cast OXCMA films, solution concentration and shear rate effects on OXCMA OFETs, HOMO and LUMO levels of PCBM, *o*-xylene, and indene C_{60} derivatives, summary of the electrical performance of OFET devices based on the drop-cast thin films, peak assignments for the out-of-plane XRD patterns. This material is available free of charge via the Internet at http://pubs.acs.org.

AUTHOR INFORMATION

Corresponding Author

*E-mail: joonhoh@unist.ac.kr (J.H.O.), bumjoonkim@kaist.ac.kr (B.J.K.). Phone: 82-52-217-2531 (J.H.O.), 82-42-350-3935 (B.J.K.).

Author Contributions

‡These authors contributed equally.

Notes

The authors declare no competing financial interest.

ACKNOWLEDGMENTS

This work was supported by National Research Foundation of Korea (NRF) grants funded by the Korean Government (MEST; Grants 2011-0026424, 2011-0017174, and 2012-0001061) and the Global Frontier Research Center for Advanced Soft Electronics (Grant 2011-0031628). This research was also supported by the New & Renewable Energy KETEP Grant 2010-T100100460 and a Fundamental R&D Program Grant for Core Technology of Materials funded by the Ministry of Knowledge Economy, Republic of Korea. H.Y. acknowledges financial support from the Global Ph.D. Fellowship funded by the NRF. The authors acknowledge Prof. Tae-Woo Lee at Postech for providing N-DMBI.

REFERENCES

(1) Zhan, X.; Facchetti, A.; Barlow, S.; Marks, T. J.; Ratner, M. A.; Wasielewski, M. R.; Marder, S. R. *Adv. Mater.* **2011**, *23*, 268−284.
(2) Wurthner, F.; Stolte, M. *Chem. Commun.* **2011**, *47*, 5109−5115.
(3) Usta, H.; Facchetti, A.; Marks, T. J. *Acc. Chem. Res.* **2011**, *44*, 501−510.
(4) Zhao, X. G.; Zhan, X. W. *Chem. Soc. Rev.* **2011**, *40*, 3728−3743.
(5) Yan, H.; Chen, Z.; Zheng, Y.; Newman, C.; Quinn, J. R.; Dotz, F.; Kastler, M.; Facchetti, A. *Nature* **2009**, *457*, 679−686.
(6) Schmidt, R.; Oh, J. H.; Sun, Y. S.; Deppisch, M.; Krause, A. M.; Radacki, K.; Braunschweig, H.; Konemann, M.; Erk, P.; Bao, Z.; Wurthner, F. *J. Am. Chem. Soc.* **2009**, *131*, 6215−6228.
(7) Hummelen, J. C.; Knight, B. W.; Lepeq, F.; Wudl, F.; Yao, J.; Wilkins, C. L. *J. Org. Chem.* **1995**, *60*, 532−538.
(8) Shaheen, S. E.; Brabec, C. J.; Sariciftci, N. S.; Padinger, F.; Fromherz, T.; Hummelen, J. C. *Appl. Phys. Lett.* **2001**, *78*, 841−843.
(9) Li, G.; Shrotriya, V.; Huang, J. S.; Yao, Y.; Moriarty, T.; Emery, K.; Yang, Y. *Nat. Mater.* **2005**, *4*, 864−868.
(10) Scharber, M. C.; Wuhlbacher, D.; Koppe, M.; Denk, P.; Waldauf, C.; Heeger, A. J.; Brabec, C. L. *Adv. Mater.* **2006**, *18*, 789−794.
(11) Padinger, F.; Rittberger, R. S.; Sariciftci, N. S. *Adv. Funct. Mater.* **2003**, *13*, 85−88.
(12) Waldauf, C.; Schilinsky, P.; Perisutti, M.; Hauch, J.; Brabec, C. J. *Adv. Mater.* **2003**, *15*, 2084−2088.
(13) Wobkenberg, P. H.; Bradley, D. D. C.; Kronholm, D.; Hummelen, J. C.; de Leeuw, D. M.; Colle, M.; Anthopoulos, T. D. *Synth. Met.* **2008**, *158*, 468−472.
(14) Tiwari, S. P.; Zhang, X.-H.; Potscavage, W. J.; Kippelen, B. *J. Appl. Phys.* **2009**, *106*, 054504.
(15) Chikamatsu, M.; Itakura, A.; Yoshida, Y.; Azumi, R.; Yase, K. *Chem. Mater.* **2008**, *20*, 7365−7367.
(16) Chikamatsu, M.; Itakura, A.; Yoshida, Y.; Azumi, R.; Kikuchi, K.; Yase, K. *J. Photochem. Photobiol. Chem.* **2006**, *182*, 245−249.
(17) Wobkenberg, P. H.; Ball, J.; Bradley, D. D. C.; Anthopoulos, T. D.; Kooistra, F.; Hummelen, J. C.; de Leeuw, D. M. *Appl. Phys. Lett.* **2008**, *92*, 143310.
(18) Chikamatsu, M.; Nagamatsu, S.; Yoshida, Y.; Saito, K.; Yase, K.; Kikuchi, K. *Appl. Phys. Lett.* **2005**, *87*, 203504.
(19) Anthopoulos, T. D.; Kooistra, F. B.; Wondergem, H. J.; Kronholm, D.; Hummelen, J. C.; de Leeuw, D. M. *Adv. Mater.* **2006**, *18*, 1679−1684.
(20) Ball, J. M.; Bouwer, R. K. M.; Kooistra, F. B.; Frost, J. M.; Qi, Y. B.; Domingo, E. B.; Smith, J.; de Leeuw, D. M.; Hummelen, J. C.; Nelson, J.; Kahn, A.; Stingelin, N.; Bradley, D. D. C.; Anthopoulos, T. D. *J. Appl. Phys.* **2011**, *110*, 014506.
(21) Kim, K. H.; Kang, H.; Nam, S. Y.; Jung, J.; Kim, P. S.; Cho, C. H.; Lee, C.; Yoon, S. C.; Kim, B. J. *Chem. Mater.* **2011**, *23*, 5090−5095.
(22) Kim, K. H.; Kang, H.; Kim, H. J.; Kim, P. S.; Yoon, S. C.; Kim, B. J. *Chem. Mater.* **2012**, *24*, 2373−2381.
(23) Kang, H.; Cho, C. H.; Cho, H. H.; Kang, T. E.; Kim, H. J.; Kim, K. H.; Yoon, S. C.; Kim, B. J. *ACS Appl. Mater. Interfaces* **2012**, *4*, 110−116.
(24) Laird, D. W.; Stegamat, R.; Richter, H.; Vejins, V.; Scott, L.; Lada, T. A. Organic photovoltaic devices comprising fullerenes and derivatives thereof. WO2008018931A2, Feb 14, 2008.
(25) He, Y.; Chen, H.-Y.; Hou, J.; Li, Y. *J. Am. Chem. Soc.* **2010**, *132*, 1377−1382.
(26) Zhao, G.; He, Y.; Li, Y. *Adv. Mater.* **2010**, *22*, 4355−4358.
(27) Cho, C. H.; Kim, H. J.; Kang, H.; Shin, T. J.; Kim, B. J. *J. Mater. Chem.* **2012**, *22*, 14236−14245.
(28) Becerril, H. A.; Roberts, M. E.; Liu, Z. H.; Locklin, J.; Bao, Z. *Adv. Mater.* **2008**, *20*, 2588−2594.
(29) Giri, G.; Verploegen, E.; Mannsfeld, S. C.; Atahan-Evrenk, S.; Kim do, H.; Lee, S. Y.; Becerril, H. A.; Aspuru-Guzik, A.; Toney, M. F.; Bao, Z. *Nature* **2011**, *480*, 504−508.

(30) Oh, J. H.; Lee, W. Y.; Noe, T.; Chen, W. C.; Konemann, M.; Bao, Z. *J. Am. Chem. Soc.* **2011**, *133*, 4204−4207.
(31) Menke, T.; Ray, D.; Meiss, J.; Leo, K.; Riede, M. *Appl. Phys. Lett.* **2012**, *100*, 093304.
(32) Li, F. H.; Werner, A.; Pfeiffer, M.; Leo, K.; Liu, X. J. *J. Phys. Chem. B* **2004**, *108*, 17076−17082.
(33) Wei, Z. M.; Xi, H. X.; Dong, H. L.; Wang, L. J.; Xu, W.; Hu, W. P.; Zhu, D. B. *J. Mater. Chem.* **2010**, *20*, 1203−1207.
(34) Wei, P.; Oh, J. H.; Dong, G.; Bao, Z. *J. Am. Chem. Soc.* **2010**, *132*, 8852−8853.
(35) Ito, Y.; Virkar, A. A.; Mannsfeld, S.; Oh, J. H.; Toney, M.; Locklin, J.; Bao, Z. *J. Am. Chem. Soc.* **2009**, *131*, 9396−9404.
(36) Jones, B. A.; Facchetti, A.; Wasielewski, M. R.; Marks, T. J. *J. Am. Chem. Soc.* **2007**, *129*, 15259−15278.
(37) Wang, Z.; Kim, C.; Facchetti, A.; Marks, T. J. *J. Am. Chem. Soc.* **2007**, *129*, 13362−13363.
(38) Oh, J. H.; Sun, Y. S.; Schmidt, R.; Toney, M. F.; Nordlund, D.; Konemann, M.; Wurthner, F.; Bao, Z. *Chem. Mater.* **2009**, *21*, 5508−5518.
(39) Li, C. Z.; Chueh, C. C.; Yip, H. L.; Zou, J. Y.; Chen, W. C.; Jen, A. K. Y. *J. Mater. Chem.* **2012**, *22*, 14976−14981.
(40) Anthopoulos, T. D.; Anyfantis, G. C.; Papavassiliou, G. C.; de Leeuw, D. M. *Appl. Phys. Lett.* **2007**, *90*, 122105.
(41) de Leeuw, D. M.; Simenon, M. M. J.; Brown, A. R.; Einerhand, R. E. F. *Synth. Met.* **1997**, *87*, 53−59.
(42) Wurthner, F. *Angew. Chem., Int. Ed.* **2001**, *40*, 1037−1039.
(43) Ie, Y.; Nishida, K.; Karakawa, M.; Tada, H.; Aso, Y. *J. Org. Chem.* **2011**, *76*, 6604−6610.
(44) Katz, H. E.; Lovinger, A. J.; Johnson, J.; Kloc, C.; Siegrist, T.; Li, W.; Lin, Y. Y.; Dodabalapur, A. *Nature* **2000**, *404*, 478−481.
(45) Oh, J. H.; Wei, P.; Bao, Z. *Appl. Phys. Lett.* **2010**, *97*, 243305.
(46) Wei, P.; Menke, T.; Naab, B. D.; Leo, K.; Riede, M.; Bao, Z. *J. Am. Chem. Soc.* **2012**, *134*, 3999−4002.
(47) Cornil, J.; Beljonne, D.; Calbert, J. P.; Bredas, J. L. *Adv. Mater.* **2001**, *13*, 1053−1067.
(48) Bredas, J. L.; Beljonne, D.; Coropceanu, V.; Cornil, J. *Chem. Rev.* **2004**, *104*, 4971−5004.
(49) Coropceanu, V.; Cornil, J.; da Silva Filho, D. A.; Olivier, Y.; Silbey, R.; Bredas, J. L. *Chem. Rev.* **2007**, *107*, 926−952.
(50) Rode, B. M. *Monatsh. Chem.* **1981**, *112*, 911−916.
(51) Kim, J.; Han, A. R.; Seo, J. H.; Oh, J. H.; Yang, C. *Chem. Mater.* **2012**, *24*, 3464−3472.
(52) Zhu, X. Q.; Zhang, M. T.; Yu, A.; Wang, C. H.; Cheng, J. P. *J. Am. Chem. Soc.* **2008**, *130*, 2501−2516.
(53) Nollau, A.; Pfeiffer, M.; Fritz, T.; Leo, K. *J. Appl. Phys.* **2000**, *87*, 4340−4343.
(54) Werner, A.; Li, F. H.; Harada, K.; Pfeiffer, M.; Fritz, L.; Leo, K.; Machill, S. *Adv. Funct. Mater.* **2004**, *14*, 255−260.
(55) Walzer, K.; Maennig, B.; Pfeiffer, M.; Leo, K. *Chem. Rev.* **2007**, *107*, 1233−1271.
(56) Ma, L.; Lee, W. H.; Park, Y. D.; Kim, J. S.; Lee, H. S.; Choa, K. *Appl. Phys. Lett.* **2008**, *92*, 063310.
(57) Li, H.; Tee, B. C.; Cha, J. J.; Cui, Y.; Chung, J. W.; Lee, S. Y.; Bao, Z. *J. Am. Chem. Soc.* **2012**, *134*, 2760−2765.